Self-supervised Pre-training for Transferable Multi-modal Perception

Xiaohao Xu, Tianyi Zhang, Jinrong Yang, Matthew Johnson-Roberson, *Member, IEEE,* Xiaonan Huang

Abstract—In autonomous driving, multi-modal perception models leveraging inputs from multiple sensors exhibit strong robustness in degraded environments. However, these models face challenges in efficiently and effectively transferring learned representations across different modalities and tasks. This paper presents NeRF-Supervised Masked Auto Encoder (NS-MAE), a self-supervised pre-training paradigm for transferable multi-modal representation learning. NS-MAE is designed to provide pre-trained model initializations for efficient and high-performance fine-tuning. Our approach uses masked multi-modal reconstruction in neural radiance fields (NeRF), training the model to reconstruct missing or corrupted input data across multiple modalities. Specifically, multi-modal embeddings are extracted from corrupted LiDAR point clouds and images, conditioned on specific view directions and locations. These embeddings are then rendered into projected multi-modal feature maps using neural rendering techniques. The original multi-modal signals serve as reconstruction targets for the rendered feature maps, facilitating self-supervised representation learning. Extensive experiments demonstrate the promising transferability of NS-MAE representations across diverse multi-modal and single-modal perception models. This transferability is evaluated on various 3D perception downstream tasks, such as 3D object detection and BEV map segmentation, using different amounts of fine-tuning labeled data. Our code will be released to support the community.

I. INTRODUCTION

Advancing robust autonomous driving relies on the integration of multi-modal perception [1], a critical area of research that combines different sensor data to enhance environmental understanding. Progress in transferable representation learning has alleviated the data demands [2] of sophisticated network architectures [3]. However, these developments have predominantly targeted single-modal systems. The pre-training of multi-modal perception models, which shows better robustness under degraded scenarios, remains an under-explored frontier.

Before delving into the design of self-supervised representation learning for multi-modal perception models, we review the fully-supervised paradigm [4]. This involves separate pre-training of LiDAR and camera networks with 3D labels. However, scalability is limited due to the scarcity of labeled data, especially the laborious task of annotating paired images and sparse LiDAR point clouds for 3D perception,
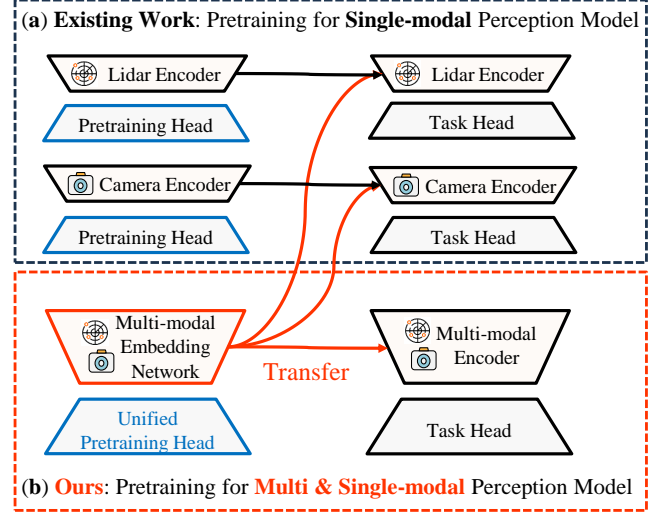
Fig. 1. **Motivation**. We aim to propose a unified self-supervised pre-training method to learn a multi-modal representation transferable to both multi-modal and single-modal perception models for autonomous driving.

leading to a dearth of high-quality 3D labels. Moreover, annotated labels cannot stimulate the learning of rich visual representations due to sparse semantics.

For single-modal perception, self-supervised pre-training methods have been proposed [5]–[7] to facilitate label-efficient transfer with either camera or LiDAR inputs (see Fig. 1a). However, **no research has delved into pre-training of multi-modal perception models for autonomous driving**, such as BEVFusion [4]. In this work, as shown in Fig. 1b, we pose the question: *Can we develop a multi-modal representation learning method that is transferable to both multi-modal and single-modal perception models?*

To this end, we consider key characteristics. Inspired by vision pre-training [2], we argue that an ideal framework should be:

- **Unified**: Versatile and applicable across diverse input modalities, architectures, and downstream tasks.
- **Scalable**: Capable of leveraging vast unlabeled multi-modal datasets and accommodating large-scale models.
- **Neat**: Streamlined and adaptable to various perception modalities.

Focusing on these objectives, we break down the design of a pre-training framework for multi-modal perception into two key sub-problems: **1**) learning transferable multi-modal representation; **2**) unifying the optimization formulation for multi-modal representation.

To foster self-supervised learning of multi-modal repre-

sentations, we draw inspiration from the Masked AutoEncoder (MAE) paradigm's remarkable success [2]. MAE's mask-then-reconstruct approach has demonstrated impressive transferability across diverse tasks. Thus, we aim to adapt MAE to acquire transferable multi-modal perception representations, thereby enhancing the capabilities of advanced multi-modal perception models [4].

To achieve a unified optimization of multi-modal representations, we utilize Neural Radiance Fields (NeRF) [8]. NeRF offer an elegant approach to encode different scene characteristics, *e.g.*, color and geometry, through a differential neural volume rendering technique. We leverage NeRF as a foundational component for multi-modal perception pretraining for two primary reasons: **1**) the imaging processes of optical systems like LiDAR and cameras can be effectively approximated by radiance field rendering; **2**) neural rendering consolidates multi-modal reconstruction through a coherent and interpretable physical model. By integrating NeRF's rendering process into perception pre-training, we facilitate the optimization of unified multi-modal representations.

We take advantage of the synergy of MAE and NeRF and propose a unified self-supervised multi-modal perception pre-training framework (NS-MAE) that elegantly learns transferable representations. As depicted in Fig. 2, we integrate plug-and-play pre-training modules (blue in Fig. 2) with the embedding network of multi-modal perception models [4] (black in Fig. 2). During the pre-training, we apply modality-specific masking to images and LiDAR point clouds, separately. Then, we send the corrupted modalities to the multi-modal embedding network for embedding extraction. Specifically, we extract the embeddings that are generated and fused in two crucial coordination systems, *i.e.*, the world and the camera coordination, for perception models [9]. Afterward, for each specific view direction and spatial sampling location, the embeddings are further rendered into diverse projected modality feature maps via differential volume rendering. Finally, the rendered feature maps are supervised by original images and point clouds via reconstruction-based self-supervised optimization. We conduct comprehensive experiments to verify the transferability of multi-modal representation learned via NS-MAE for diverse multi-modal and single-modal perception models.

In summary, the contribution of this work is as follows:

- We propose a **self-supervised pre-training framework for multi-modal representation learning** for autonomous driving, *i.e.*, NS-MAE, which can be applied to multi-modal and single-modal perception models.
- We enable both the **self-supervised learning** and **optimization unification** of transferable multi-modal representation via plug-and-play designs in the spirit of multi-modal reconstruction in the neural radiance field.
- We employ NS-MAE in various advanced single-modal and multi-modal perception models and **verify the transferability of multi-modal representation derived via NS-MAE** on diverse 3D perception tasks with diverse amounts of fine-tuning data.
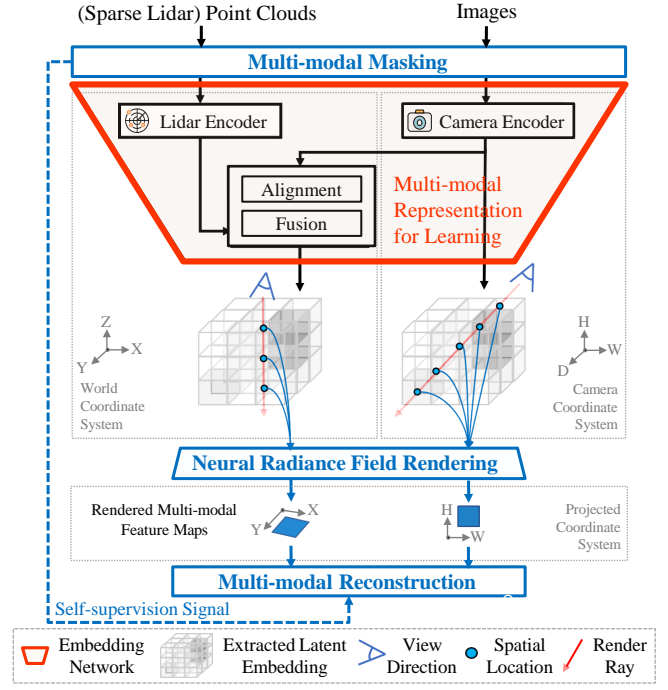

Fig. 2. **Pipeline overview of the proposed pre-training framework, *i.e.*, NS-MAE**, for multi-modal perception. Blue modules denote the proposed plug-and-play components for transferable representation learning.

II. OUR APPROACH

A. Problem Formulation of Perception Pre-training.

Given a tuple of images $\mathbf{I} = (I_1, I_2, ..., I_N \in \mathbb{R}^{H \times W \times 3})$ collected from N views with their corresponding camera parameters $(\mathbf{P}_1\mathbf{K}_1, \mathbf{P}_2\mathbf{K}_2, ..., \mathbf{P}_N\mathbf{K}_N)$ (where $\mathbf{P}$ and $\mathbf{K}$ denote camera pose and intrinsic matrix) and sparse LiDAR point clouds $\mathcal{P} = \{p_i = [x_i, y_i, z_i, r_i] \in \mathbb{R}^4\}_{i=1,...,t}$,[1] the goal of perception pretraining is to design a proxy task to learn the parameter set, *i.e.*, transferable representation, of an embedding network ϕ_{emb}, which can be used to initialize the parameter set of the downstream perception model $\phi_{down}(\supset \phi_{emb})$ for further fine-tuning.

B. Pipeline Overview

As shown in Fig. 2, the pipeline of NS-MAE pre-training includes the following three key steps to enable the transferable multi-modal perception representation learning:

1) Masking (Sec. II-D): The inputs, *i.e.*, images, and voxelized LiDAR point clouds, are separately masked;

2) Rendering (Sec. II-E): The embedding encoded from masked images and point clouds is rendered into color and projected point cloud feature maps, *i.e.*, multi-view depth maps, via neural rendering [8];

3) Reconstruction (Sec. II-G): The rendered results are optimized by the ground-truth images and point clouds

---

[1]x, y, z denotes the position of a point in the world coordinate space; the LiDAR intensity r is optional for the input but is used as common practice for the LiDAR-based encoder in perception models [10] to boost performance.

via multi-modal reconstruction-based optimization in a self-supervised learning manner.

C. Training Architecture

As shown in Fig. 2, the pre-training architecture, *i.e.*, a typical embedding network of multi-modal perception models, comprises the following components:

Camera encoder. The camera encoder takes masked images as input and generates the perspective-view (PER) image embedding $\mathbf{e}_I^{PER} \in \mathbb{R}^{H/\kappa \times W/\kappa \times D \times C}$ (κ denotes the down-sampling ratio).

LiDAR encoder. The LiDAR encoder takes masked LiDAR voxels as input and generates BEV embedding of LiDAR modality $\mathbf{e}_L^{BEV} \in \mathbb{R}^{X \times Y \times Z \times C_L}$. The encoder is typically implemented with VoxelNet [10].

Alignment module. This module aligns camera and LiDAR features by transform the perspective-view image embedding $\mathbf{e}_I^{PER}$ of camera coordination to BEV embedding $\mathbf{e}_I^{BEV} \in \mathbb{R}^{X \times Y \times Z \times C_I}$ of world coordination. Thus, image and LiDAR embeddings are aligned in the world coordination. We follow the implementation of Lift-Splat-Shoot [11].

Fusion block. The fusion block fuses the BEV embedding of camera branch $\mathbf{e}_I^{BEV}$ and LiDAR branch $\mathbf{e}_L^{BEV}$, to generate fused multi-modal BEV embedding $[\mathbf{e}_I^{BEV}; \mathbf{e}_L^{BEV}] \in \mathbb{R}^{X \times Y \times Z \times (C_I + C_L)}$ via a simple concatenation ($[\cdot; \cdot]$).

D. Multi-modal Masking

Image Masking. The original unmasked image I is first divided into regular non-overlapping image patches. Then, a random binary mask $M \in \{0, 1\}^{H \times W}$ is applied to mask out a large portion of image patches by replacing them with a learnable [MASK] token ($\in \mathbb{R}^{s \times s \times 3}$, where $s \times s$ denotes the patch size). Afterward, the image that is partially masked out is sent to the camera encoder for embedding extraction.

LiDAR Masking. After transforming the input LiDAR point cloud into its voxelized form, we mask a large fraction of non-empty voxels (70% to 90%). Then, the partially-masked voxels are processed in the LiDAR encoder to generate the LiDAR embedding.

E. NeRF-like Rendering Network

Vanilla rendering mechanism. NeRF [8] takes a set of posed images and encodes the scene with volume density and emitted radiance for the purpose of view synthesis. In NeRF, a rendering network f maps a given 3D point $\mathbf{x} \in \mathbb{R}^3$ ($\mathbb{R}^3$ denotes the scene's world space) and a particular viewing direction $\omega \in \mathbb{S}^2$ ($\mathbb{S}^2$ denotes the sphere of directions) to the differential sigma field density $\sigma \in \mathbb{R}$ and RGB color $\mathbf{c} \in \mathbb{R}^3$, like so: $f(\mathbf{x}, \omega) = (\sigma, \mathbf{c})$.

Conditional rendering network for pre-training. As our goal (representation learning) is different from the goal of vanilla NeRF (view synthesis), we leverage a reformulated rendering network design. In particular, we additionally introduce a latent multi-modal embedding $\mathbf{e}$ from the embedding network of the perception model to the inputs of the

rendering network f, like so: $f(\mathbf{x}, \omega, \mathbf{e}) = (\sigma, \mathbf{c})$. Thus, the gradient from differential rendering and the reconstruction-based self-supervision stages can be back-propagated to the embedding network for end-to-end learning.

F. NeRF-like Rendering Target

Vanilla Color Rendering. Given the pose $\mathbf{P}$ and intrinsic $\mathbf{K}$ of a *virtual camera*, we shoot rays $\mathbf{r}(t) = \mathbf{o} + t\mathbf{d}$ originating from the $\mathbf{P}$'s center of projection $\mathbf{o}$ in direction ω derived from its intrinsic $\mathbf{K}$ to render the RGB color $\hat{\mathbf{C}}(\mathbf{r})$ via standard volume rendering [12], which is formulated as:

$$\hat{\mathbf{C}}(t) = \int_0^\infty T(t)\sigma(t)\mathbf{c}(t)dt, \tag{1}$$

where $\mathbf{c}(t)$ and $\sigma(t)$ are the differential color radiance and density, and $T(t) = \exp(-\int_0^t \sigma(s)ds)$ checks for occlusions by integrating the differential density from 0 to t. Specifically, the discrete form can be approximated as:

$$\hat{\mathbf{C}}(\mathbf{r}) = \sum_{i=1}^N T_i(1 - \exp(-\sigma_i \delta_i))\mathbf{c}_i, \tag{2}$$

where N is the number of sampled points along the ray, $\delta_i = t_{i+1} - t_i$ is the distance between two adjacent ray samples and the accumulated transmittance T_i is $\exp(-\sum_{j=1}^{i-1} \sigma_j \delta_j)$.

Multi-modal rendering for pre-training. For multi-modal pre-training, the rendering targets can be extended to unleash the power of multi-modal data. In particular, apart from the color that reflects the semantics of the scene, the LiDAR ray that captures 3D geometry in the form of point clouds is also a kind of radiance. Going beyond the differential RGB color radiance $\mathbf{c}(t)$ for color rendering in Eq. (1), we leverage the differential radiance of a kind of *modality* $\mathbf{a}(t)$ for multi-modal rendering. Specifically, the rendering process to derive the projected feature map $\hat{\mathbf{A}}(t)$ can be formulated as:

$$\hat{\mathbf{A}}(t) = \int_0^\infty T(t)\sigma(t)\mathbf{a}(t)dt, \tag{3}$$

Typically, to render the projected 3D point cloud feature map, *i.e.*, 2D depth $\hat{\mathbf{D}}(\mathbf{r})$, the differential radiance of one modality, *i.e.*, $\mathbf{a}(t)$, can be set as the integration of the distance distribution field $\int_0^t dt$. Then, the discrete form to render the depth map can be expressed as:

$$\hat{\mathbf{D}}(\mathbf{r}) = \sum_{i=1}^N (T_i(1 - \exp(-\sigma_i \delta_i)) \sum_{j=1}^{i-1} \delta_j), \tag{4}$$

G. Multi-modal Reconstruction

Vanilla color reconstruction objective. Given a set of rendering rays $\mathcal{S}_r$ passing through the pixels of the original image, the goal of this step is to minimize the square of the L_2-norm of the difference between the ground truth color $\mathbf{C}(r)$ and the rendered color $\hat{\mathbf{C}}(r)$ of ray r:

$$\mathcal{L}_C = \frac{1}{|\mathcal{S}_r|} \sum_{r \in \mathcal{S}_r} \|\hat{\mathbf{C}}(\mathbf{r}) - \mathbf{C}(\mathbf{r})\|_2^2, \tag{5}$$
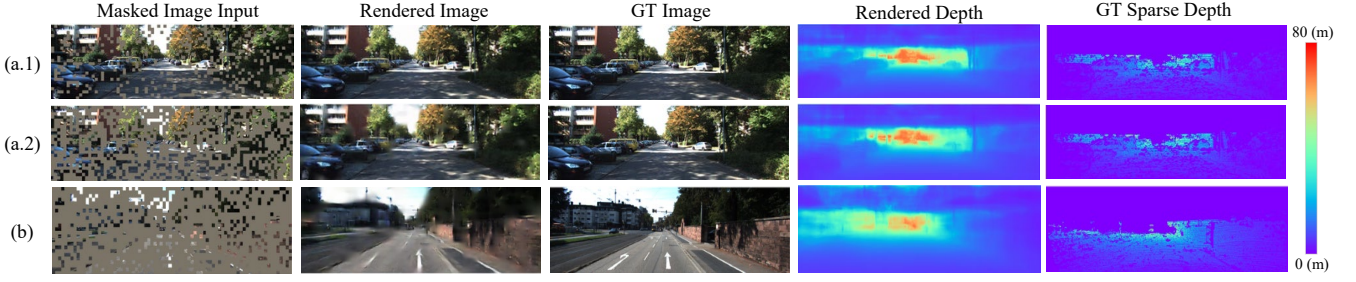
Fig. 3. **Qualitative results of perspective-view image and depth** on KITTI [13] *val* set.
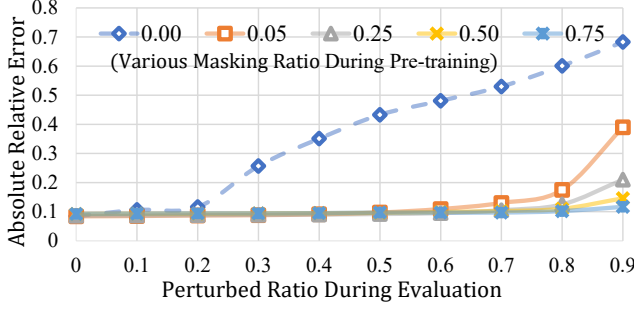

Fig. 4. **Quantitative comparisons on depth reconstruction quality** (measured by absolute relative error) on KITTI [13] *val* set with varied perturbed ratios of the input image during evaluation. Here, perturbation is implemented with random masking.
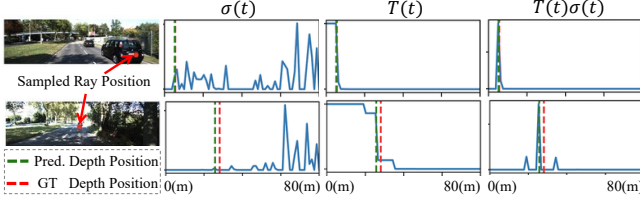

Fig. 5. **Qualitative visualizations of the radiance terms in rendering equations** (*c.f.* Sec. II-E), including volume density $\sigma(t)$, accumulated transmittance $T(t)$, and their product $T(t)\sigma(t)$, of sampled rendering rays on KITTI [13] *val*. Here, the rendering view direction is orthogonal to the perspective-view image plane.

Multi-modal reconstruction objective for pre-training. Given a set of rendering rays $\mathcal{S}_r$ passing through the ground-truth target, we minimize the L_p-norm of the difference between the ground-truth view-specific projected feature map $\mathbf{A}(r)$ and the rendered result $\hat{\mathbf{A}}(r)$ of ray r to the p-th power:

$$\mathcal{L}_{\mathrm{A}} = \frac{1}{|\mathcal{S}_r|} \sum_{r \in \mathcal{S}_r} \|\hat{\mathbf{A}}(\mathbf{r}) - \mathbf{A}(\mathbf{r})\|_p^p, \tag{6}$$

The overall objective function jointly optimize the reconstruction for multiple (K) view-specific modalities:

$$\mathcal{L} = \sum_{k=1}^{K} (\lambda_k \cdot \mathcal{L}_{\mathrm{A}_k}) \tag{7}$$

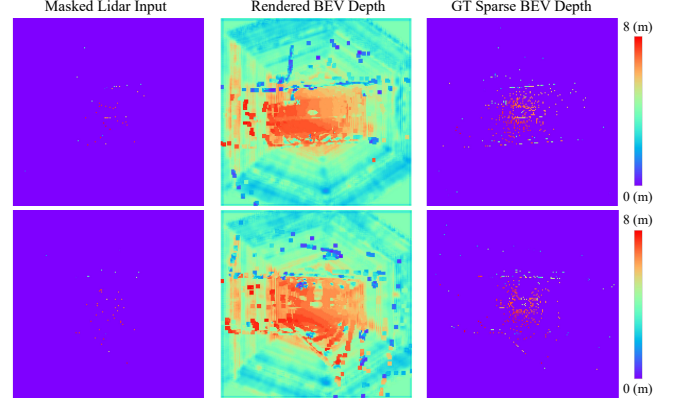λ_k indicates the coefficient to modulate the k-th sub-loss.

Fig. 6. **Qualitative results of bird's-eye-view (BEV) depth**, *i.e.*, **BEV occupancy**, rendered from a viewpoint that is orthogonal to the road plane, on nuScenes [14] *val*. **Zoom in to view better.**

H. Training Setup and Details

Training strategy. The embedding network (Sec. II-C) is pre-trained for 50 epochs. We use the AdamW [15] optimizer with a learning rate of 1e-4 and a weight decay of 0.01. Following mainstream perception models [4], [10], a one-cycle scheduler [16] is adopted. The network is trained on 8 NVIDIA V100 GPUs with a batch size of 16.

Masking. 1) For image: the masking patch size is set as 4×4 and 8×8 for images with resolutions of 128×352 and 256×704; the masking ratio is set as 50%. **2**) For LiDAR: the point cloud range is set as -54~54 (m), -54~54 (m), and -5~3 (m) for X, Y, and Z axes, respectively, and the voxel size is set as [0.075, 0.075, 0.2](m); the masking ratio of non-empty LiDAR voxel is set as 90% or in a range-aware manner [5] for single-sweep and multi-sweep point clouds.

Rendering. 1) For rendering view directions, we select two typical and critical views for 3D perception models, *i.e.*, bird's eye view (BEV) ω^{BEV} and perspective view (PER) ω^{PER}. **2**) We implement the rendering network with *conv* layers. Specifically, the rendering network first transforms the embedding $\mathbf{e} \in \mathbb{R}^{D_1 \times D_2 \times D_3 \times D_C}$ [2] extracted from the embedding network into sigma-field feature volume $V_\sigma \in \mathbb{R}^{D_1 \times D_2 \times D_3' \times 1}$ and color feature volume $V_\mathbf{c} \in$

---

[2] In the special case, when $\omega = \omega^{PER}$, dimensions D_1, D_2, D_3 refer to H, W, D axes of the camera coordination; when $\omega = \omega^{BEV}$, D_1, D_2, D_3 refer to X, Y, Z axes of the world coordination.

$\mathbb{R}^{D_1 \times D_2 \times D_3' \times 3}$, which are then processed via rendering to derive the projected feature maps for further reconstruction-based optimization. **3**) For discretized rendering functions, the parameter δ is set as 0.2 and 0.8 for the rendering in BEV and perspective view.

Reconstruction. 1) For reconstruction targets, we leverage color field map $\mathbf{C}$ which corresponds to multi-view camera-collected images, perspective-view depth $\mathbf{D}^{PER}$ which is generated by projecting LiDAR point clouds on perspective-view image planes, and BEV depth $\mathbf{D}^{BEV}$ which is generated by projecting the voxelized LiDAR point cloud on the BEV plane. **2**) We construct the set of rendering rays $\mathcal{S}_r$ with rays emitted orthogonally to the BEV plane to render depth in BEV ($\mathbf{D}^{BEV}$), and it is constructed with rays passing through image plane to render color and depth in perspective view ($\mathbf{C}$, $\mathbf{D}^{PER}$). **3**) For the parameter p in Eq. (6), we set it as 2 and 1 for color and depth, respectively. **4**) For coefficients of the color, perspective-view depth, and BEV depth, we set them as 1e4, 1e-2, and 1e-2, respectively, to normalize the numerical value of diverse modalities.

Implementation. We implement the network in PyTorch using the open-sourced MMDetection3D [17]. Data augmentations mainly follow official LiDAR and image augmentations for 3D perception models [4], [18] except the ones that require ground-truth labels, *e.g.*, database-sampler [19].

I. Remark: Properties of The Embedding Network Pre-trained by NS-MAE

In this section, we analyze the properties of the embedding network pretrained by NS-MAE.

NS-MAE induces robust multi-modal reconstruction. In Fig. 3, given the input images with diverse masking ratios, we show the rendering results of perspective-view images and projected point cloud feature maps, *i.e.*, depth maps. Case (a.1)&(a.2) of Fig. 3 shows that the multi-modal embedding network pre-trained with NS-MAE can render visually-high-quality color and depth of the scene. In Case (b) of Fig. 3, even if the input image is masked out with an extremely high masking ratio (80%), the rendered image and depth can still reconstruct coarse-level color and geometry well. To quantitatively study the robustness of the multi-modal representation pre-trained via NS-MAE, we provide the depth reconstruction results of models trained and evaluated with various masking ratios on KITTI [13]. As is shown in Fig. 4, the models trained with masked modeling exhibit better robustness to perturbations thanks to the learned modality completion and generalization ability.

NS-MAE is a physics-informed unknown-region filter. In Fig. 5, we visualize the radiance terms in rendering equations (Eq. (2) and Eq. (4) in Sec. II-E) of sampled rendering rays to understand the property of the rendering equations better. During reconstruction-based optimization (Sec. II-G), the accumulated transmittance $T(t)$ term in the prior rendering functions serves as a *band-pass filter* along the ray direction, *e.g.*, the direction from the origin (0m) to the farthest (80m) of Fig. 5. Specifically, $T(t)$ helps selectively filter out the unknown region (from the position of an object to the farthest, *i.e.*, *approximate infinity*), and only optimize *non-occupied* regions (from the origin of the ray to the object) and *occupied* regions (where objects exist), respectively. Besides, the sigma field $\sigma(t)$ term is trained to predict zero for *non-occupied* regions between the origin of the ray and the object, deriving a focused impulse in the product of accumulated transmittance and sigma field $T(t)\sigma(t)$.

NS-MAE Enhances BEV Occupancy Maps Even with sparse LiDAR input, NS-MAE pretraining reconstructs dense BEV depth, indicating object occupancy on the BEV plane. Fig. 6 shows how NS-MAE, trained with image and Li-DAR pairs, creates denser BEV occupancy maps, effectively decoupling objects along the height axis. This significantly improves BEV map segmentation performance (Sec. III-C).

III. Experiment

A. Dataset and Evaluation Metric

nuScenes [20] is a large-scale 3D perception dataset with six surrounding-view cameras and LiDAR point clouds per frame. For 3D object detection, it contains up to 1.4 million annotated 3D bounding boxes for 10 classes. The evaluation metrics are the detection score (NDS) and mean average precision (mAP). For BEV map segmentation, Intersection-over-Union (IoU) on 6 background classes and the mean IoU (mIoU) are used, limited to the [-50m, 50m] $\times$ [-50m, 50m] region around the ego car [4].

KITTI-3D [27] is a widely-used benchmark for 3D object detection, consisting of 7,481 training and 7,518 testing image-LiDAR pairs. The training set is split into *train* (3,712 samples) and *val* (3,769 samples) [27]. As a long-standing, small-scale benchmark, performance on KITTI-3D is close to saturation. Evaluation metrics include 3D IoU (AP_{3D}) and BEV IoU (AP_{BEV}) with average precision.

B. Baseline Models

BEVFusion [4] is a multi-modal perception model for 3D object detection and BEV map segmentation. It uses Swin-T [28] with FPN [29] as the Camera Encoder, VoxelNet [22] as the LiDAR Encoder, and LSS [30] for Cam2World view transformation. LiDAR point clouds are voxelized at a resolution of 0.075m for both tasks. The rendering network employs separate convolutional layers for bird's eye and perspective views.

VFF [21] (Voxel Field Fusion) is a cross-modality 3D object detection model. It uses ResNet-50 [31] as the Camera Encoder and various voxel-based LiDAR backbones, such as PV-RCNN [32] and VoxelRCNN [24]. The rendering network utilizes FPN-like convolution layers for perspective-view and simple conv 3×3 layers for BEV rendering.

BEVDet [25] is a camera-only 3D perception model using Swin-T [28] with FPN [29] as the Camera Encoder and LSS [30] for Cam2World view transformation.

CenterPoint [26] is a LiDAR-only 3D object detection model using VoxelNet [10] as the backbone for point cloud representation.

Method	Modality	#Sweep	#ImgSize	Per-class mAP										mAP	NDS
				Car	Truck	C.V.	Bus	Trail.	Barr.	Moto.	Bike	Ped.	T.C.		
BEVFusion [4]	LC	1	128×352	81.1	37.4	12.3	59.0	31.5	64.1	46.7	28.9	80.3	63.1	50.5	53.3
+ NS-MAE	LC	1	128×352	81.6	40.1	13.9	59.8	30.1	64.7	48.9	30.3	81.0	64.4	**51.5**	**54.7**
BEVFusion [4]	LC	9	256×704	87.4	40.4	25.7	67.0	38.8	71.6	68.2	48.6	85.5	74.5	60.8	64.1
+ NS-MAE	LC	9	256×704	88.1	45.9	25.1	68.8	37.2	73.8	70.8	56.6	86.9	77.4	**63.0**	**65.5**

Method	DB	AP_{BEV}			AP_{3D}		
		Easy	Moderate	Hard	Easy	Moderate	Hard
VFF-SECOND		91.71	85.77	83.54	87.25	76.44	74.02
+ NS-MAE		**92.65**	**88.24**	**85.83**	**88.25**	**78.40**	**74.37**
VFF-SECOND	✓	92.83	88.92	88.22	89.45	82.32	79.39
+ NS-MAE	✓	**93.04**	**90.43**	**88.46**	**91.48**	**82.58**	**79.77**
VFF-PVRCNN	✓	92.65	90.86	88.55	91.75	85.09	82.68
+ NS-MAE	✓	**92.94**	**91.00**	**90.49**	**92.03**	**85.31**	**83.05**
VFF-VoxelRCNN	✓	**95.67**	91.56	89.20	92.46	85.25	82.93
+ NS-MAE	✓	95.57	**91.69**	**89.23**	**92.51**	**85.59**	**82.95**

C. Main Transfer Results

In this section, we assess the effectiveness of pre-training by directly transferring it to different perception models for two common 3D perception tasks: 3D object detection and BEV map segmentation.

We follow the fine-tuning setups of baseline models and fine-tune the whole framework of them in an end-to-end manner and without using any extra data (*i.e.*, model parameters are randomly initialized). Concretely, we fine-tune models on nuScenes and KITTI-3D for 20 and 80 epochs, respectively. By default, CBGS [19] trick is not used during fine-tuning. Then, we compare the performance between models that are *without pre-training* and models whose embedding networks are *pre-trained via NS-MAE*.

1) Transfer to 3D Object Detection Task for Multi-modal Perception models: For representation transferability evaluation, we select two baseline models, *i.e.*, BEVFusion [4] and VFF [21], which represent the state-of-the-art performance for multi-modal 3D perception on nuScenes [14] and KITTI-3D benchmarks, respectively. In Table I, we show that NS-MAE can effectively boost the performance for the multi-modal model BEVFusion under various input settings, including varied LiDAR sweeps and image resolutions. Notably, for the multi-modal version of the BEVFusion model with multi-sweep LiDAR and higher image resolution (#Sweep:9, #ImgSize:256×704), *NS-MAE brings more than 2% improvement (+2.2%) in mAP and 1.4% improvement in NDS*. Moreover, in Table II, for VFF [21] framework
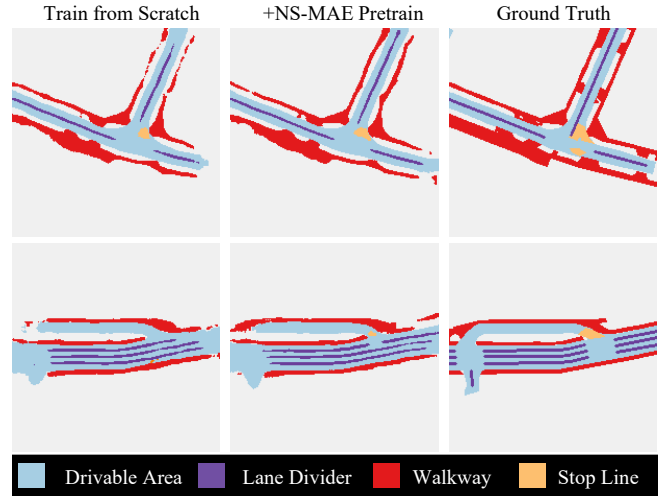

Fig. 7. **Qualitative comparisons of BEV map segmentation results** on nuScenes [14] *val* with multi-modal perception model BEVFusion [4]. Specifically, we compare the qualitative results of the model which is trained from scratch (Train from Scratch) and the results of the model which is pre-trained via NS-MAE (+NS-MAE Pretrain). The ground-truth BEV map segmentation result (Ground Truth) is provided for reference.

with various 3D detection heads, including SECOND [22], PVRCNN [23], and VoxelRCNN [24], the representation pre-trained via NS-MAE also improves the BEV and 3D detection performance in nearly all sub-metrics over training from scratch.

2) Transfer to 3D Object Detection Task for Single-modal Perception models: In Table III, we show the generality of pre-trained representation via NS-MAE to be transferred to single-modal, *i.e.*, camera-only and LiDAR-only, perception models. For the camera-only perception model BEVDet [25], *NS-MAE brings more than 2% NDS improvement* for the settings of both the default (20) and doubled (2×: 40) training epochs. For the LiDAR-only baselines [26], [33], the transferable representation learned via our NS-MAE consistently shows its effectiveness. Moreover, compared to Voxel-MAE [5] that targets pre-training for the LiDAR-only perception models, our NS-MAE that targets unified pre-training for multi-modal perception models shows better performance (62.1% *v.s.* 61.4% in NDS) for the LiDAR-only baseline, CenterPoint [26].

3) Transfer to BEV Map Segmentation Task: As is shown in Table IV, NS-MAE largely boosts the performance

Method	Modality	#Sweep	#ImgSize	Per-class mAP										mAP	NDS
				Car	Truck	C.V.	Bus	Trail.	Barr.	Moto.	Bike	Ped.	T.C.		
BEVDet [25]	C	/	256×704	35.3	15.7	2.7	**18.2**	5.5	31.0	19.8	18.3	26.9	46.0	21.9	29.4
+ NS-MAE	C	/	256×704	**37.1**	**18.0**	**3.6**	18.0	**7.0**	**41.3**	**20.3**	**19.8**	**28.1**	**47.6**	**24.1**	**32.1**
BEVDet$^{2\times}$ [25]	C	/	256×704	37.1	16.4	2.7	18.9	5.8	42.0	20.7	18.3	28.3	49.0	23.9	31.8
+ NS-MAE	C	/	256×704	**38.3**	**17.9**	**4.5**	18.3	**8.1**	**47.1**	**21.5**	**18.8**	**29.4**	**49.8**	**25.4**	**33.9**
CenterPoint [26]	L	9	/	80.9	52.4	14.4	64.0	29.6	58.7	59.4	45.6	80.4	60.8	54.6	61.3
+ VoxelMAE [5]	L	9	/	80.6	**53.7**	13.7	63.2	29.2	**61.1**	**60.5**	45.4	80.4	61.1	54.9	61.4
+ NS-MAE	L	9	/	**81.2**	53.0	**14.7**	63.7	**30.2**	60.0	60.1	**47.1**	**81.6**	**61.3**	**55.3**	**62.1**

Method	Modality	Per-class IoU						mIoU
		Dri.	P.C.	Walk.	S.L.	Car.	Div.	
BEVFusion [4]	LC	75.0	42.6	52.6	24.4	26.6	36.0	42.9
+ NS-MAE	LC	**78.0**	**45.9**	**55.5**	**26.1**	**35.4**	**38.9**	**46.6**
BEVDet [25]	C	72.7	35.6	44.7	21.1	34.0	32.3	40.1
+ NS-MAE	C	**76.1**	**39.9**	**49.0**	**23.5**	**41.6**	**35.6**	**44.3**

Method	Metric	Sampling Ratio			
		1%	5%	10%	100%
Label-Efficient regime 3D object detection					
BEVFusion [4]	mAP	26.2	46.1	54.2	60.8
+ NS-MAE	mAP	**30.2**	**47.6**	**55.9**	**63.0**
BEVFusion [4]	NDS	44.2	55.4	60.3	64.1
+ NS-MAE	NDS	**45.4**	**57.0**	**61.4**	**65.5**
Label-Efficient regime BEV map segmentation					
BEVFusion [4]	mIoU	29.7	39.4	41.3	42.9
+ NS-MAE	mIoU	**31.1**	**41.6**	**45.1**	**46.6**

Setting	Masking	Rendering Tagets			mAP	NDS
		C	$\mathbf{D}^{PER}$	$\mathbf{D}^{BEV}$		
Baseline					50.5	53.3
(A1)		✓			50.2	53.9
(A2)	✓	✓			50.7	54.2
(B1)	✓		✓		50.9	54.2
(B2)	✓			✓	51.0	54.3
(B3)			✓	✓	49.6	52.8
(B4)	✓		✓	✓	51.3	54.4
Default	✓	✓	✓	✓	**51.5**	**54.7**

D. Label-Efficient Transfer Results

Efficient transfer (*e.g.*, fewer annotations) on downstream tasks brings about great application value to real-world scenarios. Thus, we evaluate both label-efficient regime 3D detection and BEV segmentation on nuScenes. Specifically, nuScenes training split is sampled with different ratios (1% to 10%) to generate label-efficient fine-tuning datasets. For fair comparisons, all models are end-to-end fine-tuned for the same iterations as the default fine-tuning setting (100%).

In Table V, ***our pre-training schema shows the best performance under all settings of sampling ratios of labeled fine-tuning data*** for both 3D object detection and BEV-map segmentation tasks, demonstrating good label-efficient transferability of the representation pre-trained via NS-MAE.

E. Ablation Study

We ablate the components of NS-MAE in Table VI and provide the following insights about how to learn transferable multi-modal representation for perception via NS-MAE.

Masking of input modalities is critical for effective representation learning. *Without masking:* When rendering the feature maps of color and depth without masking (settings (A1) and (B3)) for representation learning, the transferred performance could be even worse than the baseline setting (Baseline). *With masking:* When enabling the multi-modal masking for the inputs, the comparison between settings

for BEV map segmentation. Specifically, our pre-training schema (NS-MAE) yields a significant improvement of approximately 4% in mIoU for both the multi-modal and camera-only perception models compared to the baseline setting. Notably, NS-MAE brings better segmentation quality for all classes. Fig. 7 compares the BEV map segmentation results of two models: one *trained from scratch* and the other *pre-trained using the NS-MAE* schema [4], which demonstrate that the transferred representation from NS-MAE enhances the segmentation quality for 3D perception.

(A2)(B1)(B2) with the baseline (Baseline) verifies the effectiveness of masked reconstruction of the feature map of color and projected point cloud, *i.e.*, depth.

Rendering with more modalities and more view directions encourages more transferable representation. *More modalities:* When multi-modal masking is enabled, the comparisons between each setting of (A2)(B2)(B3) and the baseline (Baseline) verify the effectiveness of each rendering target ($\mathbf{C}$, $\mathbf{D}^{PER}$, and $\mathbf{D}^{BEV}$). *More view directions:* As point clouds lie in the 3D space, rendered feature maps of projected point clouds ($\mathbf{D}$) in diverse views can be simultaneously optimized in a self-supervised manner. When rendering the projected feature maps of point clouds with more views for reconstruction-based optimization (B4), the performance can be further boosted compared to using only a single view direction ((B1) or (B2)). Finally, by incorporating all rendering targets above with multi-modal masking used, the default setting of NS-MAE (Default) achieves the best performance with 1.5% higher NDS and 1.0% higher mAP than the baseline setting due to their mutual benefits.

IV. CONCLUSION AND FUTURE WORK

We have proposed a unified self-supervised pre-training paradigm (NS-MAE) for multi-modal perception models. Specifically, NS-MAE conducts masked multi-modal reconstruction in NeRF to enable transferable multi-modal representation learning in a unified and neat fashion. Extensive experiments demonstrate the encouraging transferability and generalization of the learned representation via NS-MAE for both multi-modal and single-model perception models.

Limitation and future work. Although we have not yet explored NS-MAE with larger models and data due to computation and time limitations, it is an important avenue for future investigation. To evaluate the scalability of the pre-training strategy, it would be beneficial to incorporate larger-scale autonomous driving datasets such as Argoverse [34].In addition, we focus on the RGB image and LiDAR depth modalities. However, we believe that NS-MAE can be potentially extended to other sensors relevant to self-driving, such as radar and ultrasonic sensors. Additionally, enhancing the view selection for neural rendering-based reconstruction holds potential in further improving the quality of the learned representation.

REFERENCES

[1] S. Ettinger, S. Cheng, B. Caine, C. Liu, H. Zhao, S. Pradhan, Y. Chai, B. Sapp, C. R. Qi, Y. Zhou *et al.*, "Large scale interactive motion forecasting for autonomous driving: The waymo open motion dataset," in *ICCV*, 2021.

[2] K. He, X. Chen, S. Xie, Y. Li, P. Dollár, and R. Girshick, "Masked autoencoders are scalable vision learners," in *CVPR*, 2022.

[3] A. Vaswani, N. M. Shazeer, N. Parmar, J. Uszkoreit, L. Jones, A. N. Gomez, L. Kaiser, and I. Polosukhin, "Attention is all you need," in *NeurIPS*, 2017.

[4] Z. Liu, H. Tang, A. Amini, X. Yang, H. Mao, D. Rus, and S. Han, "Bevfusion: Multi-task multi-sensor fusion with unified bird's-eye view representation," in *ICRA*, 2023.

[5] C. Min, D. Zhao, L. Xiao, Y. Nie, and B. Dai, "Voxel-mae: Masked autoencoders for pre-training large-scale point clouds," *arXiv preprint arXiv:2206.09900*, 2022.

[6] A. Boulch, C. Sautier, B. Michele, G. Puy, and R. Marlet, "Also: Automotive lidar self-supervision by occupancy estimation," in *CVPR*, 2023, pp. 13 455–13 465.

[7] H. Yang, T. He, J. Liu, H. Chen, B. Wu, B. Lin, X. He, and W. Ouyang, "Gd-mae: generative decoder for mae pre-training on lidar point clouds," in *CVPR*, 2023, pp. 9403–9414.

[8] K.-A. Aliev, A. Sevastopolsky, M. Kolos, D. Ulyanov, and V. Lempitsky, "Neural point-based graphics," in *ECCV*, 2020.

[9] Z. Li, W. Wang, H. Li, E. Xie, C. Sima, T. Lu, Y. Qiao, and J. Dai, "Bevformer: Learning bird's-eye-view representation from multi-camera images via spatiotemporal transformers," in *ECCV*, 2022.

[10] Y. Zhou and O. Tuzel, "VoxelNet: End-to-end learning for point cloud based 3d object detection," in *CVPR*, 2018.

[11] J. Philion and S. Fidler, "Lift, Splat, Shoot: Encoding images from arbitrary camera rigs by implicitly unprojecting to 3d," in *ECCV*, 2020.

[12] J. T. Kajiya and B. P. Von Herzen, "Ray tracing volume densities," *ACM SIGGRAPH computer graphics*, 1984.

[13] A. Geiger, P. Lenz, and R. Urtasun, "Are we ready for autonomous driving? the kitti vision benchmark suite," in *CVPR*, 2012.

[14] H. Caesar, V. Bankiti, A. H. Lang, and et al., "nuscenes: A multimodal dataset for autonomous driving," in *CVPR*, 2020.

[15] I. Loshchilov and F. Hutter, "Decoupled weight decay regularization," *arXiv preprint arXiv:1711.05101*, 2017.

[16] L. N. Smith and N. Topin, "Super-convergence: Very fast training of neural networks using large learning rates," *arXiv preprint arXiv:1708.07120*, 2017.

[17] M. Contributors., "Mmdetection3d: Open-mmlab next-generation platform for general 3d object detection," *https://github.com/open-mmlab/mmdetection3d*, 2020.

[18] T. Liang, H. Xie, K. Yu, Z. Xia, Z. Lin, Y. Wang, T. Tang, B. Wang, and Z. Tang, "BEVFusion: A Simple and Robust LiDAR-Camera Fusion Framework," in *NeurIPS*, 2022.

[19] B. Zhu, Z. Jiang, X. Zhou, Z. Li, and G. Yu, "Class-balanced grouping and sampling for point cloud 3d object detection," *arXiv preprint arXiv:1908.09492*, 2019.

[20] H. Caesar, V. Bankiti, A. H. Lang, S. Vora, V. E. Liong, Q. Xu, A. Krishnan, Y. Pan, G. Baldan, and O. Beijbom, "nuScenes: A multimodal dataset for autonomous driving," in *CVPR*, 2020.

[21] Y. Li, X. Qi, Y. Chen, L. Wang, Z. Li, J. Sun, and J. Jia, "Voxel field fusion for 3d object detection," in *CVPR*, 2022.

[22] Y. Yan, Y. Mao, and B. Li, "Second: Sparsely embedded convolutional detection," *Sensors*, 2018.

[23] S. Shi, C. Guo, L. Jiang, Z. Wang, J. Shi, X. Wang, and H. Li, "Pv-rcnn: Point-voxel feature set abstraction for 3d object detection," in *CVPR*, 2020.

[24] J. Deng, S. Shi, P. Li *et al.*, "Voxel r-cnn: Towards high performance voxel-based 3d object detection," in *AAAI*, 2021.

[25] J. Huang, G. Huang, Z. Zhu, and D. Du, "Bevdet: High-performance multi-camera 3d object detection in bird-eye-view," *arXiv preprint arXiv:2112.11790*, 2021.

[26] T. Yin, X. Zhou, and P. Krähenbühl, "Center-based 3d object detection and tracking," in *CVPR*, 2021.

[27] X. Chen, K. Kundu, Y. Zhu *et al.*, "3d object proposals for accurate object class detection," in *NeurIPS*, 2015.

[28] Z. Liu, Y. Lin, Y. Cao, H. Hu, Y. Wei, Z. Zhang, S. Lin, and B. Guo, "Swin transformer: Hierarchical vision transformer using shifted windows," in *ICCV*, 2021.

[29] T.-Y. Lin, P. Dollár, R. Girshick, K. He, B. Hariharan, and S. Belongie, "Feature pyramid networks for object detection," in *CVPR*, 2017.

[30] J. Philion and S. Fidler, "Lift, splat, shoot: Encoding images from arbitrary camera rigs by implicitly unprojecting to 3d," in *ECCV*, 2020.

[31] K. He, X. Zhang, S. Ren, and J. Sun, "Deep residual learning for image recognition," in *CVPR*, 2016.

[32] S. Shi, C. Guo, L. Jiang *et al.*, "Pv-rcnn: Point-voxel feature set abstraction for 3d object detection," in *CVPR*, 2020.

[33] X. Bai, Z. Hu, X. Zhu, Q. Huang, Y. Chen, H. Fu, and C.-L. Tai, "Transfusion: Robust lidar-camera fusion for 3d object detection with transformers," *arXiv preprint arXiv:2203.11496*, 2022.

[34] B. Wilson, W. Qi, T. Agarwal, J. Lambert, J. Singh, S. Khandelwal, B. Pan, R. Kumar, A. Hartnett, J. K. Pontes *et al.*, "Argoverse 2: Next generation datasets for self-driving perception and forecasting," *arXiv preprint arXiv:2301.00493*, 2023.